Adsorption reverse electrodialysis driven by power plant waste heat to generate electricity and provide cooling

Adsorption reverse electrodialysis driven by power plant waste heat to generate electricity and provide cooling

C. Olkis[a]*, S. Brandani[a] and G. Santori[a]

[a] *The University of Edinburgh, School of Engineering, Institute for Materials and Processes, Sanderson Building, The King's Buildings, Mayfield Road, EH9 3FB Edinburgh, Scotland, UK*

*Corresponding author: colkis@ed.ac.uk

HIGHLIGHTS

- Waste heat as low as 40 °C converted into electricity
- System provides cooling to the steam cycle process
- Experiments proving that silica gel can be regenerated at 40 °C
- Experimentally validated model for each component
- Improving the performance ratio of adsorption desalination PR > 1
- Exergy efficiency up to 15 % for waste heat at 40 °C

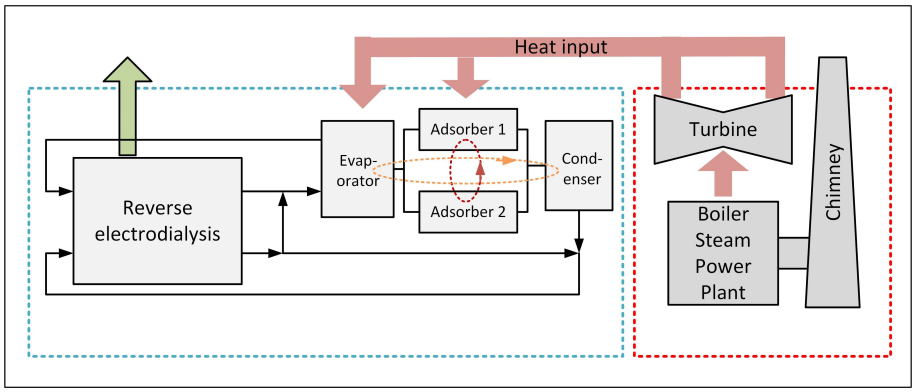

ABSTRACT

Steam power plants release more than half of the primary energy input as ultra low temperature heat below 40 °C into the environment causing thermal pollution. The emitted heat has a very low exergy content making it challenging to use as heat input by another process. Adsorption desalination combined with reverse electrodialysis can be powered by this heat and convert it into electricity. Thus, the system can mitigate thermal pollution and generate electricity at the same time. This study combines a validated reverse electrodialysis model with a dynamic adsorption desalination model that is validated with experimental data within this work. The experiments were conducted using a small-scale adsorption desalinator and silica gel proving the feasibility of the regeneration at heat source temperatures as low as 40 °C. The simulations of the integrated system analyse different heat integration scenarios showing exergy efficiencies up to 15 % and energy efficiencies up to 0.55 %. Hence, the system could generate 65 kW electricity

from a 20 MW heat source considering pumping losses.

Keywords:
Adsorption desalination, Reverse electrodialysis, Low grade heat recovery, Heat-to-Power, Steam power plant, Rankine cycle

---

1 Introduction

Power generation relies heavily on the availability of water as thermoelectric power plants are responsible for 40 % of all freshwater withdrawals in the United States [1]. Thermoelectric power plants can be cooled by open-loop systems, which withdraw water from a river source, the water runs once through the system and is returned to the river leading to thermal pollution [1]. An alternative are closed-loop systems recirculating water in cooling towers [2] with heights of up to 200 m and ground diameters of more than 120 m [3]. Closed-loop systems are economically a less attractive option compared to open-loop systems, but it is unclear if enough water will still be available for open-loop systems in the future, because of increased river temperatures due to climate change [4] and water scarcity [5]. Currently, the capacity of power plants is reduced by up to 19 % in Europe and 16 % in the United States during summers [6]. In the future, this issue will get worse since the average river water temperature will increase by up to 2.3 °C during summer in Europe as well as the United States [6]. In Europe heat emission to the surface water is regulated in various ways, depending on the ecological conditions and factors such as: the sensitivity of the receiving surface water, the local climatic conditions and the capacity of the receiver to accommodate thermal loads. From 1971-2000, the discharge limits were already exceeded for 23 days/year on average in southern Europe. The number of days are projected to increase to 44-48 days/year by 2040 and 59-82 days by 2080 [6]. Thus, there is a strong need to find economically viable alternatives to open-loop cooling, improve closed-loop cooling and in the best case to recover the waste heat flow.
The low pressure steam from the turbine of a coal fired power plant is condensed around 40 °C [7]. This heat is available at such a low regeneration temperature that it is very challenging to use it. The second largest quantities of waste heat are available below 50 °C and are solely emitted by power plants [8]. Venkatesan et al. proposed a flash cooling desalination system using the condensing heat to produce fresh water with a recovery ratio of 0.49 % [9]. The condensing heat of the power plant could also be converted into electricity, but the low temperature of 40 °C represents a challenge. Organic Rankine Cycles [10] usually utilise waste heat 100-300 °C [11, 12], although regeneration temperatures as low as 80 °C [13] and 85 °C [14] have been reported. Stirling engines [15] operate by cyclic expansion and compression of a working fluid (e.g. helium) and are driven by a temperature gradient. Commonly, Stirling engines require heat sources 120-900 °C and can achieve energy efficiencies up to 25 % [16, 17]. Studies have reported small-scale ultra-low temperature Stirling engines driven by only a few degrees [18], but energy efficiencies remain below 0.1 % [19]. McGinnis et al. proposed an osmotic heat engine using Pressure Retarded Osmosis *(PRO)*, which converts a salt gradient into pressure first and then into electricity [20]. The osmotic heat engine combined a PRO membrane with a distillation

column in a simulation. They showed that exergy efficiencies of up to 16 % are possible with a waste heat temperature of 50 °C and ambient temperature of 25 °C. They reported that the system could be driven by heat sources 40-100 °C. However, a temperature difference between ambient and heat source of at least 20 °C is required [20], but the model is not experimentally validated. In another configuration, the osmotic heat engine features a membrane distillation unit in-stead of a distillation column [21].

A similar concept is the combination of a Reverse Electrodialysis membrane *(RED)* [22] with thermal desalination [23]. RED has an advantage over PRO as it can directly convert the salt gradient into electricity without converting it into pressure first. The combination of RED with several regeneration methods has been proposed: multi-effect distillation *MED* [24, 25], thermolytic salts [26], membrane distillation *MD* [27] and adsorption desalination *AD* [28]. Micari et al. presented a modelling analysis combining validated models of RED and MD [29]. The study reports the maximum exergy efficiency of the processes at 2 % using current technology and a waste heat source of 80 °C [29]. Future improvements of the system are projected to enhance the exergy efficiency to 16.5 % at 80 °C as future membrane distillation units are reported to have a Specific Thermal Consumption $STC < 100$ kWh/m^3 [29]. Dow et al. tested a pilot membrane distillation plant powered by low grade heat ≤ 40 °C [30]. Their analysis showed that MD can operate at low temperatures, but the permeate flux is reduced by 75 % compared to operation at 60 °C [30]. In addition, Dow et al. reported experimental STC ≈ 1500 kWh/m^3 for all experiments and temperatures [30].

Adsorption desalinators evolved from adsorption chillers [31, 32] and achieve performance ratios up to 0.75 at 50 °C [33, 34], which can be converted to STC ≥ 850 kWh/m^3. In addition, adsorption reverse electrodialysis can achieve exergy efficiencies of up to 45 % with an optimal adsorption material and salt combination at a waste heat temperature of 60 °C as shown in a thermodynamic analysis [28]. However, Thu et al. have proven the feasibility of adsorption desalination at waste heat sources as low as 50 °C [34] and they have shown that the lower regeneration temperature reduces the water production of system, while the energy efficiency remains unchanged [34]. However, no other experimental study has regenerated the adsorbent below 50 °C yet as shown in table 1.

Table 1: Low temperatures used during adsorption and desorption in water adsorption experimental studies on desalination and cooling applications.

Authors	**Material**	$\mathbf{T_{ads}}$ **[°C]**	$\mathbf{T_{des}}$ **[°C]**	**Ref.**
This study	Silica gel	25	40	-
Thu et al.	Silica gel	27.6	50	[34]
Zhang et al.	Silica gel	27	55	[35]
Myat et al.	FAM Z01	29.5	55	[36]
Saha et al.	Silica gel	30	55	[37]
Woo et al.	Silica gel	20-30	65	[38]
Mitra et al.	Silica gel	36	65	[39]
Pan et al.	Silica gel	30	70	[40]
Qian et al.	Zeolite	28-34	70	[41]
Freni et al.	SWS-8L	30	77	[42]
Wu et al.	Silica gel	20	80	[43]
Chen et al.	Silica gel	31.6	82	[44]
Tso et al.	13X/CaCl2	31	85	[45]
Alsaman et al.	Silica gel	30	90	[46]
Sapienza et al.	Silica gel	28	90	[47]
Al-Dadah et al.	MOFs	30	90	[48]
Youssef et al.	CPO-27Ni	15	95	[49]

There remains a need to show that silica gel can be regenerated below 50 °C where vast quantities of waste heat are available. The possibility of ultra-low temperature regeneration would be a striking feature of adsorption desalination that enables the utilisation of adsorption for waste heat recovery from power plant condensers. Few technologies are capable to use the condensation heat efficiently.

This study investigates the combination of an adsorption reverse electrodialysis system for the generation of electricity from low-grade heat at temperatures as low as 40 °C. The study extends and continues the work presented in a preceding publication [28] where the feasibility of the process was investigated from a thermodynamic point of view neglecting all system limitations. Here, the system performance was analysed that can be achieved with current technology considering major limitations by using validated models for reverse electrodialysis and adsorption desalination. The reverse electrodialysis section of the model is adapted from Tamburini et al. [50]. Experiments were conducted using a small scale adsorption desalinator and silica gel. The experiments aim to prove for the first time that silica gel can be regenerated using ultra-low waste heat sources as low as 40 °C. The experimental results are used to validate a dynamic, lumped-parameter adsorption desalination model within this work. The validation of each of the model components allows a realistic prediction of the performance of the overall process. Moreover, a novel heat integration scheme is applied to boost the energy efficiency.

2 The adsorption reverse electrodialysis process

Fig. 1 shows the application of adsorption reverse electrodialysis *ADRED* [28] to a power plant for conversion of waste heat to power.

The system circulates a high and a low salinity solution between the RED stack and the AD re-

generation. The working principle of an adsorption desalinator is described in detail in [51, 52]. The two solutions $F_{high,in}$ and $F_{low,in}$ enter the RED unit, where electricity is generated by exploiting the salt gradient. Afterwards, the salinity gradient needs to be restored in the adsorption desalinator by partially evaporating water from the inlet flow F_2 in the AD evaporator. This water vapour is adsorbed by the silica gel in the adsorber beds. For desorption, the silica gel needs to be heated releasing water vapour that is condensed producing the distillate flow F_4, which dilutes the low salinity solution $F_{low,out}$ from the RED system in Fig. 1.

A sensible heat storage water tank is connecting ADRED to the power plant's steam cycle. The sensible heat storage unit acts as alternative heat sink for the power plant condenser, where it can reject all or part of the condensation heat instead of using the external heat sink in Fig. 1. The sensible heat of the storage unit is used for desorption of the adsorber beds. Desorption is an endothermic process that cools the heat storage unit in return. Additional cooling can be provided from the evaporator. Hence, evaporator and desorption take up condensation heat from the steam cycle reducing the load for the external heat sink. The external heat sink is also connected to the condenser and adsorber during adsorption, where it provides cooling, but at a lower temperature level than the power plant condenser. The two heat integration schemes reduce the load to the external heat sink from the ADRED system. Instead of cooling the heat storage unit, the evaporator can be heat-integrated with the condenser making the condenser independent of the external cold sink.

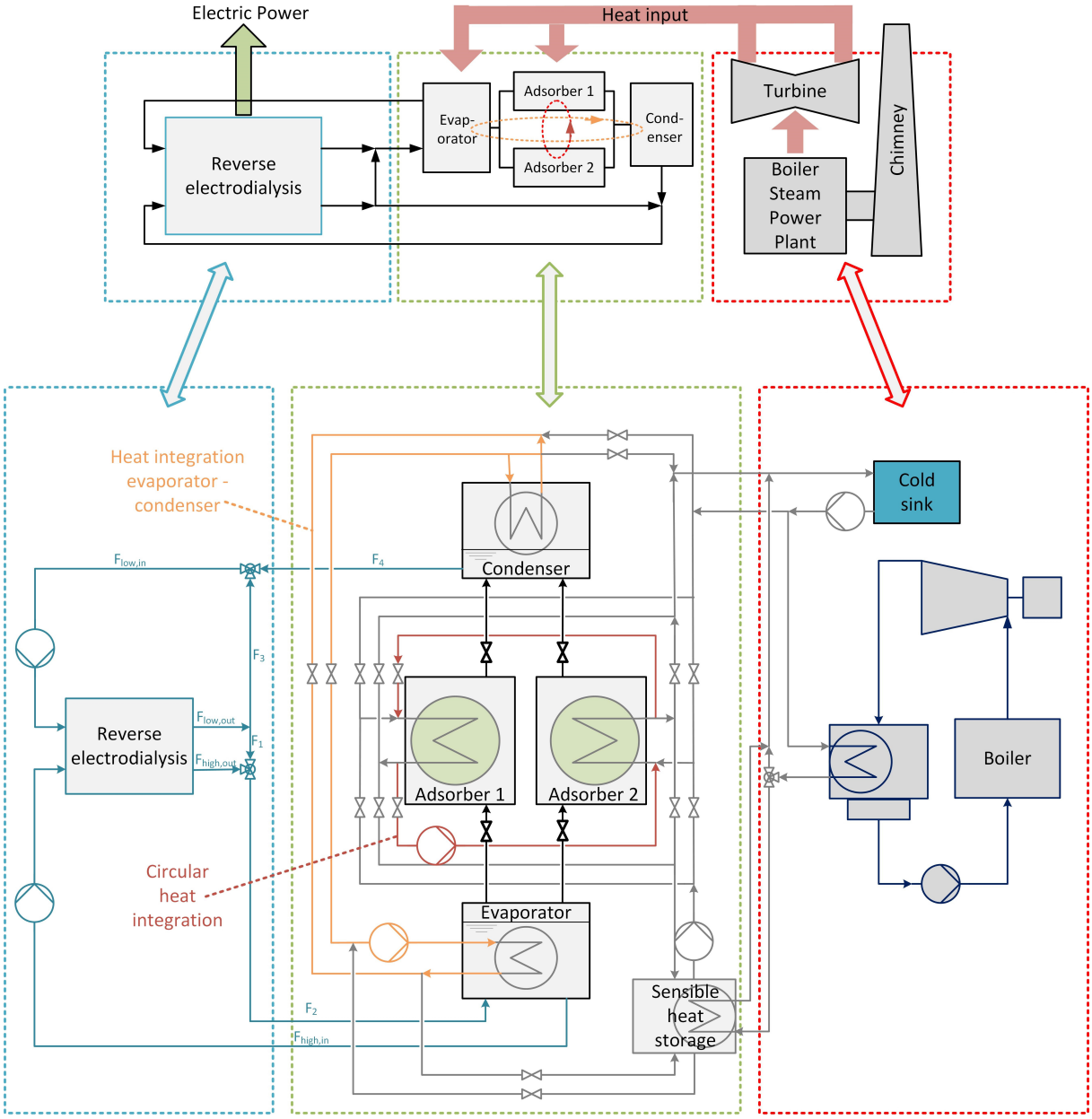

Figure 1: The ADRED system uses the condensation heat of the steam cycle to regenerate the adsorption beds. The produced distillate F_4 is used to restore the salt gradient between two saline solutions F_{high} and F_{low}. A reverse electrodialysis stack generates electricity from this salt gradient.

2.1 Modelling assumptions

A validated, dynamic model is used to investigate the heat integration scenario that achieves the best efficiency and the highest power density. The RED section of the model has been validated for aqueous sodium chloride solutions [50]. Therefore, sodium chloride was the only salt investigated here. Siogel silica gel (Oker Chemie GmbH, Germany) is a commercial material that has been fully characterised experimentally in an AD system and was chosen for this study. The model assumes:

- Homogeneous temperatures in all vessels and adsorption beds;

- Only pure water evaporates, while all salt remains in the evaporator [28];
- The salt concentration in the solution supplied from the evaporator to the membrane varies, because of the changing evaporation rate [52]. The adsorption desalination model takes the change of concentration into account, but the membrane model is steady-state and to save computation time the average salt concentration is used in each cycle;
- All components of the system are adiabatic;
- Ambient temperature $T_{cond,in}$ is 25 °C, unless otherwise specified;
- Average conditions for solutions and cell pair variables between inlet and outlet of the RED membrane as the model is independent of x-y-z-dimensions;
- Solvent flow and polarisation phenomena in the RED membrane are neglected [50]. However, the model of Tamburini et al. is experimentally validated and the modelling results match the experimental results, which they obtained with commercial RED membranes using NaCl solutions up to 5 mol/kg [50].;
- Ideal current distribution in RED membrane [50];
- The adsorbent mass of the adsorption desalinator is kept constant, while the membrane area is variable. This allows RED to cope with different distillate flow rates achieved under different conditions.
- The entire system operates under vacuum, which is provided from the steam cycle condenser ejector. This allows continuous operation of RED stack and adsorption desalination as opposed to the batch desalination process presented by Micari et al. which represents an alternative in the process design [29]

The Pitzer model and Reverse electrodialysis model are adapted from Pitzer and Mayorga [53] and Tamburini et al. [50] respectively and are reported in the appendix along with the mass balances.

2.2 Mathematical model for high performance adsorption desalination

El-Dessouky and Ettouney presented a fully heat integrated adsorption vapour compression *ADVC* system in a simplified mathematical model [54] achieving high desalination performances due to heat integration between the adsorbers. Other studies have investigated the circular heat recovery scheme of El-Dessouky and Ettouney for adsorption chillers [55, 56] finding it not beneficial. Fig. 2 highlights the differences between circular heat integration in adsorption chillers and desalinators. During circular heat integration, cooling water is cooled by the first bed and the endothermic heat of desorption 1→3, while it is heated by the second bed and the exothermic heat of adsorption 4→6, which is at a higher temperature at this point.
Circular heat integration can be applied until the temperature of both beds equilibrated in points 3 and 6 in Fig. 2. At this point, in desalination half the water up-take is desorbed, whereas in cooling only a fraction of water is desorbed due to preliminary isosteric heating and cooling phases. However, the heat of desorption is the main contributor to the energy requirement, while isosteric heating and cooling only changes the sensible heat of the system. Therefore, circular heat integration appears more promising for desalination than chilling as it can be seen in Fig

2b. As indicated in Fig. 2b, ADRED can provide an alternative to a large cooling tower as it can reduce the external cooling load by about 50 % using circular heat integration, while it still requires a heat sink. In addition, the temperature level of the released heat is reduced from 40 °C to ambient temperature during adsorption.

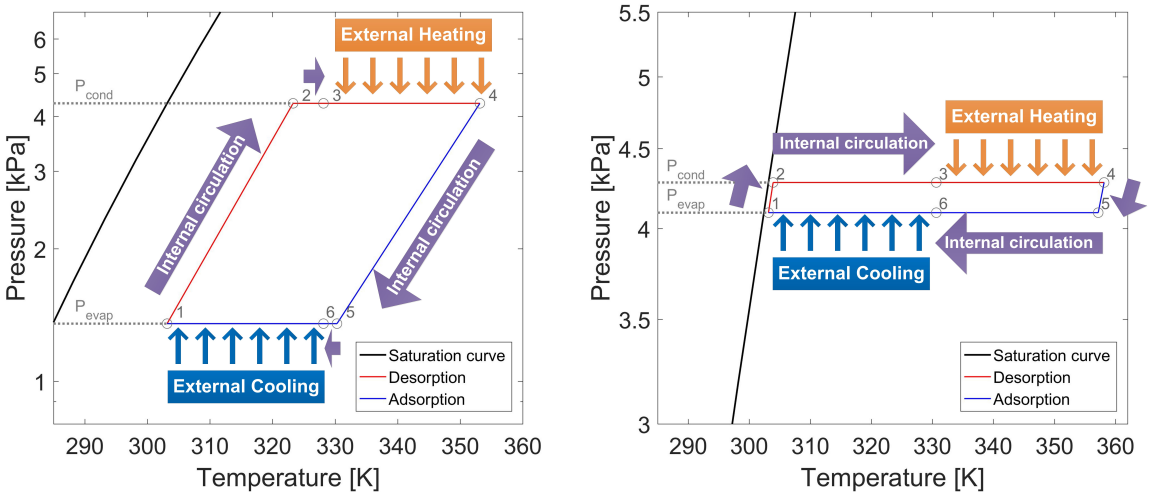

(a) (b)

Figure 2: Circular heat integration: (a) in chillers only a fraction of water is desorbed; (b) in desalination it halves the external energy input during desorption

A lumped parameter, dynamic model [57, 58] was adapted for the interpretation of the experimental adsorption desalinator and updated with the heat integration scheme of El-Dessouky. Table 2 shows the two additional phases II and IV required for internal circulation, which are added to the established sequence [59]. Table 3 shows sequence parameters used to adjust the modelling equations according to the phases in table 2. All parameters used in the model are given in table 4.

Table 2: The six phases of the adsorption desalination cycle

Phase	**Cycle**	**Bed 1**	**Phase Bed 2**	**Bed 2**	**Energy source**
I	1 → 2	Isosteric Heating	4 → 5	Isosteric Cooling	Internal circulation
II	2 → 3	Desorption	5 → 6	Adsorption	Internal circulation
III	3 → 4	Desorption	6 → 1	Adsorption	External source
IV	4 → 5	Isosteric Cooling	1 → 2	Isosteric Heating	Internal circulation
V	5 → 6	Adsorption	2 → 3	Desorption	Internal circulation
VI	6 → 1	Adsorption	3 → 4	Desorption	External source

Table 3: Values for a subset of modelling parameters for each phase of the adsorption cycle as shown in table 2

Phase	**I**	**II**	**III**	**IV**	**V**	**VI**
τ_1	0	1	1	0	0	0
τ_2	0	0	0	0	1	1
ω	0	1	1	0	1	1
ξ	0	0	1	0	0	1

The water uptake of the Siogel silica gel is assessed by Dubinin Astakhov (DA) isotherms [60, 61]:

$$q^* = q_0 \; exp\left(-\left[\frac{RT}{E} ln\left(\frac{p_{sat}}{p}\right)\right]^n\right) \tag{1}$$

The adsorption kinetics are analysed by the linear driving force (LDF) equation:

$$\frac{dq_{1/2}}{dt} = \omega_{1/2} \; \frac{15 D_{s0} \; exp(\frac{-E_a}{RT})}{R_p^2} \; (q^* - q) \tag{2}$$

The mass balances of the condenser and evaporator are shown below:

$$\frac{dM_{evap}}{dt} = -M_{sg}\left(\tau_1 \frac{dq_1}{dt} + \tau_2 \frac{dq_2}{dt}\right) + F_2 - F_{high,in} \tag{3}$$

$$\frac{dM_{cond}}{dt} = M_{sg}\left(\tau_2 \frac{dq_1}{dt} + \tau_1 \frac{dq_2}{dt}\right) - F_4 \tag{4}$$

The salt mass fraction w_{evap} in the evaporator changes according to:

$$\frac{w_{evap}}{dt} = \frac{-w_{evap}}{M_{evap}} \; \frac{dM_{evap}}{dt} + F_2 \; w_2 - F_{high,in} \; w_{high,in} \tag{5}$$

The energy balance for the evaporator is:

$$(M_{hxev} c_{p,hx} + M_{evap} c_{p,sol,evap}) \frac{dT_{evap}}{dt} = \left(\tau_1 \frac{dq_1}{dt} + \tau_2 \frac{dq_2}{dt}\right) M_{sg} L_w + \dot{m}_{evap} c_p (T_{evap,in} - T_{evap,out}) \tag{6}$$

Where M_{hxev} is the mass of the heat exchanger [kg], the latent heat L [kJ/kg], $c_{p,hx}$ is the specific heat of the aluminium heat exchanger [kJ/(kgK)] and $c_{p,w}$ is the specific heat of the cooling water [kJ/(kgK)]. $C_{p,sol,w}$ is the specific heat of the solution inside the evaporator, which is about 3.3 kJ/(kgK) for concentrated NaCl solutions at ambient temperature [62].
The energy balance of the condenser is:

$$(M_{hxco} c_{p,hx} + M_{cond} c_{p,w,cond}) \frac{dT_{cond}}{dt} = \left(\tau_2 \frac{dq_1}{dt} + \tau_1 \frac{dq_2}{dt}\right) M_{sg} L_w + \dot{m}_{cond} c_{p,w} (T_{cond,in} - T_{cond,out}) \tag{7}$$

The energy balance for the adsorbers are:

$$(M_{sg}c_{p,sg} + M_{hx,ads}c_{p,hx,ads} + M_{w,ads}c_{p,w,ads})\frac{dT_{ads1}}{dt} = \Delta h_{ads}M_{sg}\frac{dq_1}{dt} + \\ +\dot{m}_{ads}c_{p,w}[\xi\ (T_{ads2,out} - T_{ads1,out}) + (1-\xi)(T_{ads,in} - T_{ads1,out})] \quad (8)$$

$$(M_{sg}c_{p,sg} + M_{hx,ads}c_{p,hx,ads} + M_{w,ads}c_{p,w,ads})\frac{dT_{ads2}}{dt} = \Delta h_{ads}M_{sg}\frac{dq_2}{dt} + \\ +\dot{m}_{ads}c_{p,w}[\xi\ (T_{ads1,out} - T_{ads2,out}) + (1-\xi)(T_{ads,in} - T_{ads2,out})] \quad (9)$$

All outlet temperatures $T_{i,out}$ [K] are determined by the logarithmic mean temperature difference:

$$T_{out} = T + (T_{in} - T)\ exp\left(\frac{-UA}{\dot{m}_{hx}\ c_{p,w}}\right) \quad (10)$$

Where U is the overall heat transfer coefficient [W/(m^{2}K)], T is the temperature inside the vessel [K], A is the surface area of the heat exchanger [m^2] and $\dot{m}_{hx}$ is the flow rate of water supplied to the heat exchanger [kg/s]. The heat of adsorption Δh_{ads} [kJ/kg] is derived from Clausius-Clapeyron and the DA isotherm [63], where $\Theta = q_1/q_0$:

$$\Delta h_{ads} = L_w + E\ ln\left(\frac{1}{\Theta}\right)^{1/n} + \frac{E\alpha T}{n}\left(\frac{1}{\Theta}\right)^{-(n-1)/n} \quad (11)$$

Table 4: Simulation parameters for the small-scale adsorption desalinator [64] and Siogel silica gel.

Property	**Unit**	**Value**	**Reference**
$\dot{m}_{evap}$	L/min	0.4	-
$\dot{m}_{cond}$	L/min	0.8	-
$\dot{m}_{ads/des}$	L/min	0.4	-
$M_{hxev}c_{p,hx}$	kJ/K	0.137	-
$M_{hxco}c_{p,hx}$	kJ/K	0.378	-
$M_{hxads}c_{p,hx,ads}$	kJ/K	0.546	-
UA_{ads}	W/K	14	this work (exp)
UA_{cond}	W/K	7	this work (exp)
UA_{evap}	W/K	40	this work (exp)
t_{cycle}	s	1200-4000	-
R_p	m	0.002	-
M_{sg}	kg	0.21	[64]
$c_{p,sg}$	kJ/(kgK)	0.65	[65]
D_{sO}	m^2/s	$2.5{\cdot}10^{-4}$	[52]
E_a	J/mol	$4.2{\cdot}10^{-4}$	[52]
q_0	kg/kg	0.38	[66]
E	kJ/kg	220	[66]
n	-	1.1	[66]
R	J/(molK)	8.314	[67]

The two main performance indicators in adsorption desalination are the Specific Daily Water

Production $SDWP$ [$kg_w/(kg_{sg}d)$] and Performance Ratio PR [-]:

$$SDWP = N_c \int_0^{t_{cycle}} \frac{\dot{Q}_{cond}}{L_w \cdot M_{sg}} dt \tag{12}$$

$$PR = \int_0^{t_{cycle}} \frac{\dot{m}_{dist} \cdot L_w}{\dot{Q}_{des}} dt \tag{13}$$

where $\dot{Q}_{des}$ and $\dot{Q}_{cond}$ [kJ/s] are assessed through energy balances around the heat exchangers for both, simulation and experimental data:

$$\dot{Q}_{des} = \dot{m}_{hot}\ c_{p,hot}\ (T_{des,in} - T_{des,out}) \tag{14}$$

$$\dot{Q}_{cond} = \dot{m}_{cond}\ c_{p,ambient}\ (T_{cond,in} - T_{cond,out}) \tag{15}$$

where $\dot{m}_{hot/cond}$ [kg/s] are the flow rates supplied to the heat exchangers, c_p is the specific heat capacity [kJ/(kg K)] and $T_{des/cond,in/out}$ [K] represents the temperature differences between inlet and outlet of the desorber and condenser heat exchangers respectively.

3 Model analysis

3.1 Adsorption model validation for low temperature regeneration

The lumped parameter, dynamic model was validated with experimental data obtained from the small scale adsorption shown in Fig. 3a. The system features four main vessels: evaporator, condenser and two adsorbers filled with 210 g of silica gel each. Each vessel is equipped with a pressure transducer (WIKA Alexander Wiegand SE & Co. KG, Germany 0.25 %), T-Type thermocouples (Omega UK, 0.4 % accuracy) and a heat exchanger (RC Racing Radiators, Italy). The inlet and outlet temperature of the water supplied to the heat exchangers are measured with additional T-Type thermocouples and the flow rate to the heat exchangers is assessed with rotameters (Nixon Flowmeters, UK, 1.6% accuracy). The experimental system is described in detail in [64].

The sequence in table 2 was adapted to represent the physical system by skipping the internal circulation phases. Three low temperature experiments were performed to fit the model on the parameter UA [W/K] of each vessel. The experiments were conducted by slightly heating the evaporator to achieve $P_{evap} \approx P_{cond}$ [68] with $T_{cond,in} = 25$ °C, while $T_{evap,in} > T_{cond,in}$, 1200 s half cycle time and 90 s heat recovery/switching time. Fig. 3 shows the temperature curves and distillate production of the experiment at $T_{hot,in} = 40$ °C highlighting that silica gel can be regenerated at 40 °C.

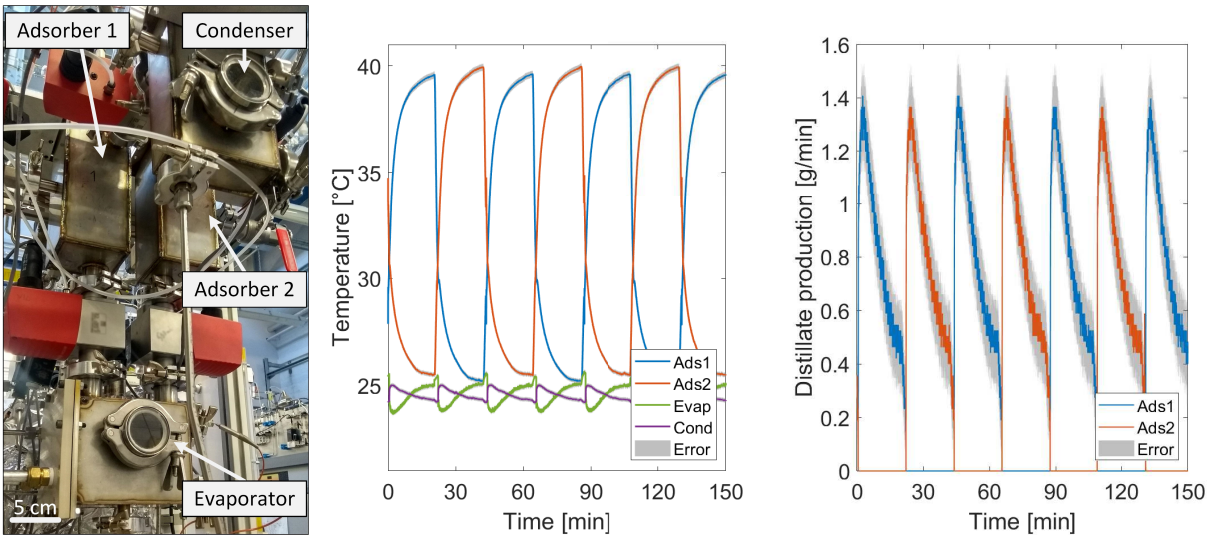

(a) (b) (c)

Figure 3: ((a) The small scale experimental system used for model validation.
b) Experimental temperature curves for $T_{evap,in}$ = 29 °C, $T_{cond,in}$ = 25 °C and $T_{hot,in}$ = 40 °C, half cycle time 1200 s and heat recovery time 90 s.
(c) Distillate production curves derived from temperature measurements of the same experiment at $T_{hot,in}$ = 40 °C.

The best fitting parameters representing the experiments are UA_{ads} = 14 W/K, UA_{cond} = 7 W/K and UA_{evap} = 40 W/K. The parameters correspond to the actual, small-scale system. The model was fitted on the system performance in terms of PR and SDWP as shown in Fig. 4. In Fig. 4a the PR for the lowest regeneration temperature is in very good agreement with the model, while for the two higher temperatures it slightly over-predicting them within the experimental error. The SDWP in Fig. 4b is over-predicted for the lowest regeneration temperature, while the two higher temperatures are in line with the experimental results. However, fitting the model on all experimentally obtained temperatures, pressures and time combinations with a single set of UA leads to considerable mismatches and deviations in some of the results. One of the main limitations of the lumped parameter, dynamic model lies in the assumption homogeneous temperatures throughout the units, whereas real systems are characterised by temperature distributions (e.g. up to 10 °C measured in the evaporator). By contrast, several authors have reported excellent agreement between the model and the experimental results [52, 46], which cannot be confirmed by this study. Based on this study, it can be concluded that the model is appropriate for system design, but only satisfactory to represent an experimental system in detail.

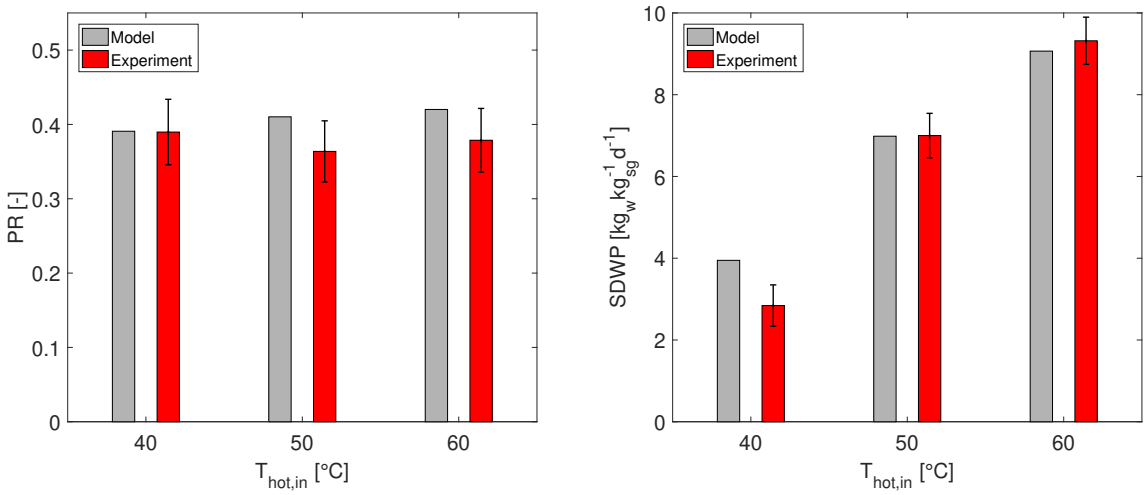

Figure 4: Experimental validation of the dynamic adsorption model for the PR (a) and the SDWP (b).

3.2 Circular heat integration to boost the performance ratio

The PR of eq. (13) quantifies the energy efficiency of the adsorption desalination system. Large thermal desalination systems like multi effect distillation can achieve PR $\approx$ 10 [69], which means they generate ten times more water per unit of energy than simple distillation. However, these systems are very large. Adsorption desalinators are more compact, have lower investment costs [52], but achieve PR $<$ 1, where Ng. et al. have reported up to PR = 0.75 in an experimental study [52]. The performance ratio of experimental systems was addressed in early studies [70]. Much recent work focused on maximising the SDWP through material design, while the PR of even the most advanced systems remained constant around 0.6 to 0.75 [52]. However, for commercial applications it is essential to develop the technology beyond PR $>$ 1, which requires an optimised process design with favourable heat exchanger to adsorption material weight ratios [71] as well as a more advanced heat integration within the system.

Fig. 5 highlights the potential of adsorption desalination with internal circulation for different internal circulation times. The internal circulation times of phase II and V in table 2 were varied from 0-1400 s, while phases III + VI were kept constant at 600 s each and phases I + IV at 30 s. Moreover, the inlet temperatures in Fig. 5 are $T_{evap,in} = T_{cond,in} = 30$ °C and $T_{hot,in} = 80$ °C. The starting point of the investigation in Fig. 5 is zero internal circulation time, which resembles the experimental system [64] without the proposed internal circulation and only a simple heat recovery described in [64]. At zero internal circulation time ($t_{ads,int} = 0$ s), the model and the experimental result are in agreement (Fig. 5). When, $t_{ads,int}$ is increased up to 1400 s, the PR increases from PR = 0.60 up to 1.04, which is an improvement of 75 % compared to the experimental result. This indicates that adsorption desalinators can exceed the threshold of PR $\geq$ 1, which is imperative for the commercial success of adsorption desalination. However, the SDWP decreases with increasing $t_{ads,int}$ as the total cycle time increases with $t_{ads,int}$. Therefore, the optimal performance is a trade-off between the two indicators. An increased PR indicates

increased energy efficiency, while a decreased SDWP implies a greater amount of silica gel and larger system footprint.

The relatively low SDWP of silica gel between 4-8 $kg_w/(kg_{sg}d)$ highlights the need for new adsorption materials that can significantly increase the SDWP and decrease the footprint with it. For example, Askalany et al. presented novel Ionogels, which are ionic liquids impregnated on a solid support structure, e.g. silica gels [72] or activated carbons [73]. Moreover, improved heat exchanger designs [71] with larger UA-parameters would reduce the cycle time and increase the SDWP as well.

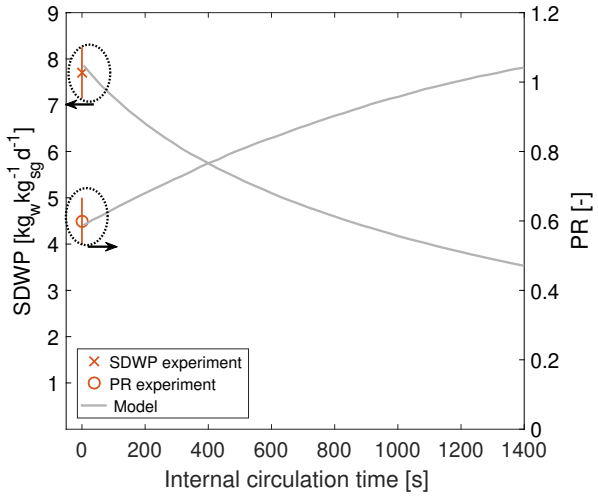

Figure 5: The model predicts that increasing internal circulation times can boost the PR above the threshold of PR=1 (a), while sacrificing the SDWP (b). The experiment is conducted without internal circulation with $T_{hot,in}$ = 80 °C, $T_{evap,in}$ = $T_{cond,in}$ = 30 °C, 600 s half cycle time and is used to validate the model.

Ng et al. have investigated the impact of the salinity on the performance [52]. They showed that the performance ratio is unaffected by the presence of salt in the evaporator, while the SDWP is decreased by less than 10 % [52]. Hence, the experiment in Fig. 5 was conducted with salt free water in the evaporator to minimise the risk of corrosion, while the salinity in the model was 35 g/kg (≈ 0.6 mol/kg) for seawater [74].

3.3 Performance of the validated adsorption reverse electrodialysis model

The model assesses the energy efficiency η_{en} and exergy efficiency η_{ex} of the ADRED process depending on the heat source temperature for each case. Moreover, it determines the SDWP and PR for the adsorption side of the system. $P_{d,ADRED}$ is calculated from eq. (57) and $P_{el,ADRED}$ from eq. (58) leading to the mass of silica gel M_{sg} = $P_{el,ADRED}/P_{d,ADRED}$. The results are compared for 6 different degrees of heat integration shown in table 5 to find the best configuration for each case.

Table 5: Different scenarios and input parameters for the ADRED model. "c-e int." = Heat integration evaporator-condenser; "circ." = Circular heat integration. The heat integration scenarios are indicated in Fig. 1. For all cases t_{ads} = 600 s and t_{isos} = 30 s.

Scenario	**Description**	$\mathbf{T_{evap,in}}$ **[°C]**	$\mathbf{t_{ads,int}}$ **[s]**
1x	No heat integration	30	1
1y	Short circ.	30	600
1z	Long circ.	30	1200
2x	No circ. + c-e int.	-	1
2y	Short circ. + c-e int.	-	600
2z	Long circ. + c-e int.	-	1200

The input conditions of the steam power plant ($T_{ads,in}$ = 40 °C) are used by the validated small-scale model to assess the process performance. The first three scenarios in table 5 consider external evaporator heating, while the last three feature heat integration between evaporator and condenser. Within each category, the sub-scenarios xyz test the suitability of the internal circulation for this application.

Fig. 6a shows that the PR of the AD side increases with the degree of heat integration. Overall, the PR is less than 1 because the working capacity of silica gel is reduced at 40 °C compared to 80 °C in Fig. 6a. However, the fully heat integrated system (scenario 2z) achieves PR = 0.63, which is 64 % higher than the PR with no heat integration in scenario 1x. The energy efficiency of scenarios 1xyz is below 2xyz in Fig. 6b, because the evaporator heating in cases 1xyz requires additional heat input, which is accounted for in the energy efficiency. The silica gel power density in Fig. 7 is highest for the system with no heat integration 1x, because it achieves the highest SDWP. Heat integration increases the cycle time, which has a negative impact on the performance as fewer cycles can be performed within one day at long cycle times.

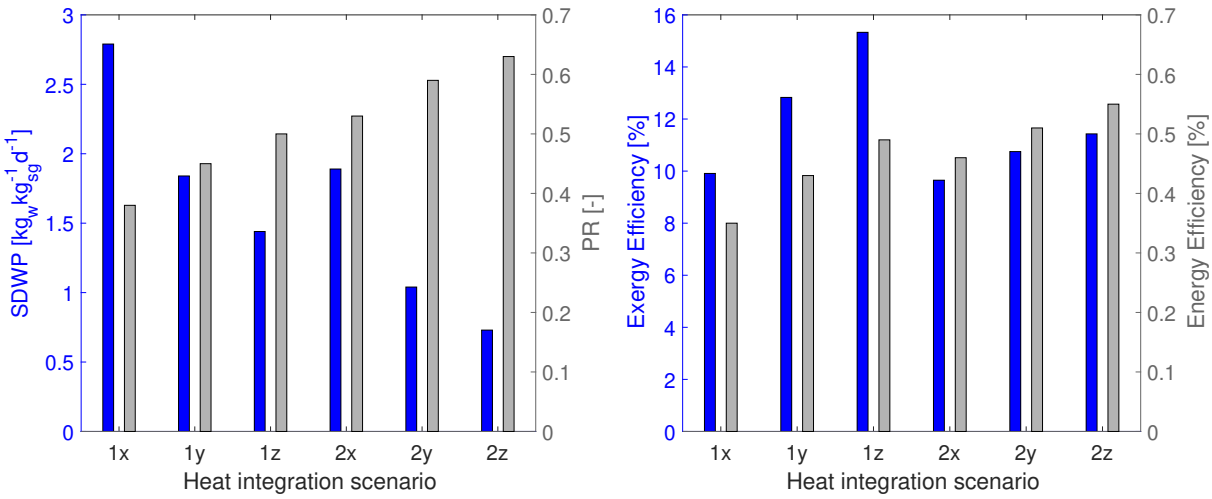

(a) (b)

Figure 6: Predicted performance of the ADRED system with input conditions from table 5:
(a) PR and SDWP of the adsorption desalination system for different heat integrations.
(b) The energy and exergy efficiency of the overall ADRED system.

The exergy efficiency in Fig. 6b is highest at 15.3 % for scenario 1z, where the evapora-

tor is heated externally and the internal circulation time is maximised. The Carnot factor ($= 1 - T_{cond,in}/T_{evap/hot,in}$) in eq. (56) is used to convert the energy efficiency to the exergy efficiency. The Carnot factor is 2.9 times lower for $T_{evap,in}$ = 30 °C than it is for $T_{hot,in}$ = 40 °C at $T_{cond,in}$ = 25 °C. Thus, heating the evaporator does not impair the exergy efficiency, because of the lower Carnot factor at 30 °C. Instead, the higher working capacity of the silica gel increases the exergy efficiency of 1xyz above 2xyz for each respective scenario. The working capacity of the material increases with evaporator heating, which is represented by the higher SDWP in 1xyz compared to 2xyz in Fig. 6a. The power density of the silica gel material is predicted between 0.2-0.7 W_{el}/kg_{sg} as shown in Fig. 7. The power density is strongly linked to the SDWP which is below 3 $kg_w/(kg_{sg}d)$ in all heat integration scenarios due to the low regeneration temperature of 40 °C.

The power density could be further improved by novel adsorption materials with higher SDWP and working capacities, future developments in heat integration and the development of improved RED membranes. The thermodynamic analysis in the preceding publication showed that highly concentrated LiCl solutions (20 mol/kg) could improve the exergy efficiency to more than 40 % [28], but this is impossible to achieve with current membranes, which are optimised for sodium chloride solutions. The ADRED system could also provide cooling as useful output by switching the material from silica gel to AQSOA Z01/Z02 [75], which are commercial zeolites [76] that maintain a constant SDWP even at low evaporator temperatures [77].

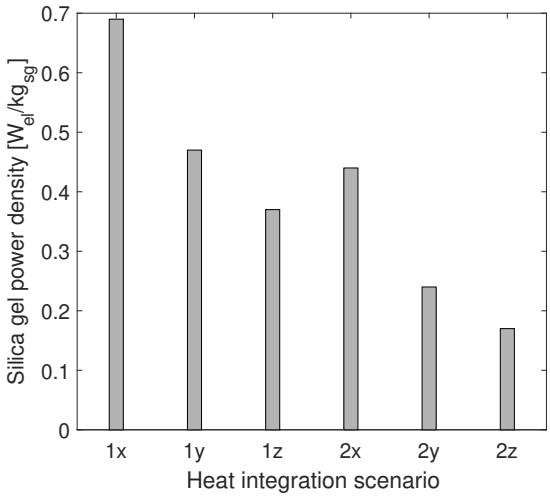

Figure 7: Predicted electric power output per kg of silica gel for the overall system.

3.4 Limitations and considerations for industrial applications

Rankine cycles can vary in sizes ranging from a few hundred kilowatt in organic Rankine cycles to gigawatts from nuclear power plants. Here, we assume a 10 MW Rankine cycle turbine is assumed with an efficiency of 33 % emitting 20 MW of waste heat that can be used to power the ADRED system. Fig. 8 uses the modelling results to estimate the system size and electricity output.

The best trade-off between size, electricity output and without external heat sink is scenario 2x, which does not feature the internal circulation. Therefore, the cycle times can be shorter

leading to an improved distillate production. From Fig. 8, the ADRED system could produce 92 kW of electricity requiring 200 tons of silica gel.

Pumping losses of about 5 kJ_{el}/kg_{w} are estimated to be lost in an AD plant in a presented by Ng et al. [52]. The distillate flow rate from the industrial scale ADRED plant is $SDWP \cdot M_{sg}$ = 4.4 kg_w/s resulting in pumping losses of 22 kW for the AD side of the system. An additional 5 % of the electricity are lost to pumping in the RED plant [50, 78]. Thus, the ADRED system generates 65.4 kW net electricity leading to an energy efficiency of 0.33 % and exergy efficiency of 7.1 %.

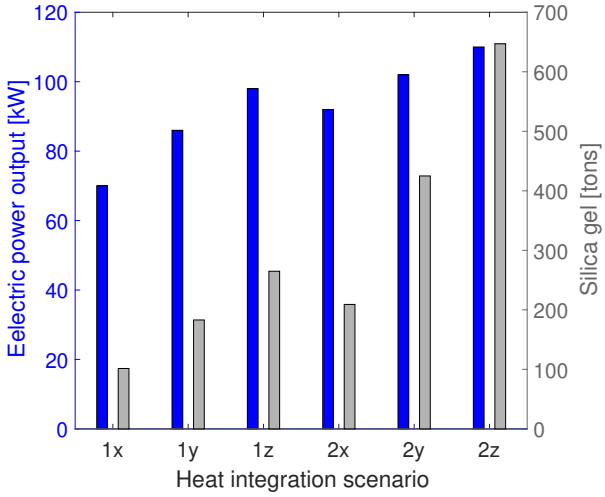

Figure 8: Predicted scale and electric power output for an industrial application

Novel adsorption materials with higher working capacities could reduce the footprint of the system as smaller adsorption beds could produce the same amount of distillate. One challenge in material selection is the working capacity from the material's equilibrium curves that can be achieved at 40 °C. Most novel materials that have been proposed for adsorption desalination showing high water capacities require regeneration temperatures well above 40 °C, e.g. MOF materials (90 °C) [79, 80] or zeolites AQSOA Z01 and Z02 (60 °C and 80 °C) [76, 77]. Ionogels show outstanding performances at regeneration temperatures as low as 25 °C. Hence, ionogels would be ideal for the ADRED process [72, 81, 82].

The amount of adsorption material could be reduced by a factor of four [81] to about 50 tons by using ionogels instead of silica gel in scenario 2x or 25 tons in scenario 1x. This would correspond to 2.5-5 $tons_{ig}$/MW. However, silica gel is an inexpensive, established commercial material, while ionogels are still under development. Moreover, silica gel remains the benchmark material for low grade heat studies despite progresses in material development [34, 83].

Another important aspect is adsorption material stability to ensure low maintenance cost, which is given for commercial materials [84]. Henninger et al. have tested the cycle stability of adsorption materials commonly used for water adsorption. They found a reduced uptake of silica gel by 5% after continuous cycling [84]. Dengler and Krückels investigated the water adsorption properties of silica gel over a period of 500 cycles [85]. They found that the equilibrium concentration and apparent diffusion coefficient are decreasing by 20 % within the first 100 cycles and plateauing. However, the two properties are not following below this limit until 500 cycles are

reached. Dengler and Krückels conclude that thermal swings change the pore structure of silica gel within the first 100 cycles, but afterwards silica gel remains stable [85].
Corrosion is another aspect that needs to be addressed in an industrial design. Demisters between evaporator and adsorber could prevent salt-water droplets to reach the adsorber and condenser together with the pure water vapour. Hence, corrosion would only be a problem in the evaporator. Hence, at least the heat exchangers of the evaporator would have to be made of stainless steel. In addition, corrosion can also occur in the pipework and valves between the RED stack and the adsorption desalinator, which needs to be addressed in the final design.
RED plant performances using highly concentrated salt solutions will be reduced by permselectivity and concentration polarisation. Concentration polarisation occurs when the concentration on the membrane-solution interface is different to the bulk concentration [86]. This leads to a reduced driving force between the low and high salinity solutions, which reduces the energy generation as well [86]. In a techno-economic analysis, Weiner et al. have identified concentration polarisation as one of the main contributors to overall membrane resistance [87]. Guerri et al. report that higher Reynolds numbers can reduce limiting effects of concentration polarisation [88]. Permselectivity is another limiting factor of RED membranes, where anion exchange membranes (AEM) and cation exchange membranes (CEM) are stacked alternatingly. Ideally, only anions can pass AEMs, while only cations pass CEMs leading to a permselectivity of 100 % [89]. However, the permselectivity is reduced at high concentrations and different salts [90]. Therefore, it is crucial to address both phenomena when designing membranes for large scale applications as presented within this study.

4 Conclusions

Steam power plants emit large amounts of waste heat at very low temperatures leading to thermal pollution of rivers and the environment. This study proposes the application of an Adsorption Reverse Electrodialysis system that uses the condensation heat of a steam power plant of 40 °C as waste heat source to convert this energy into electricity. The analysis is the continuation and further development of a preceding study that presented the concept of Adsorption Reverse Electrodialysis for the first time. The exergy content of heat emitted at 40 °C is very low and even an ideal process cannot exceed an energy efficiency of 4.8 % according to the Carnot factor.
The analysis is conducted with a simulation tool, where each component is experimentally validated. Experiments using a small scale adsorption desalinator and silica gel provided novel experimental data showing that silica gel can be regenerated at 40 °C achieving an SDWP of 2.8 $kg_w/(kg_{sg}d)$. The results were applied to validate the model. The experimental performance ratio was PR_{exp}≈0.4-0.6, which can be boosted above the threshold of PR=1 at higher temperatures and circular heat integration as indicated by the simulations. The validated reverse eletrodialysis and adsorption desalination models were combined and analysed for the input conditions of a steam cycle emitting waste heat at 40 °C. The investigation screened six different heat integration schemes achieving exergy efficiencies 10-15 % and energy efficiency of 0.35-0.55 %. In addition, the results showed that the different heat integration scenarios improve the energy efficiency, but increase the system size at the same time. Consideration for a

system scale up showed that 20 MW of waste heat could be converted into 92 kW of electricity including internal pumping losses. Future work should therefore address the application of novel materials that can be regenerated below 40 °C to decrease the system size.

Acknowledgements

This work was performed within the RED-Heat-to-Power project (Conversion of Low-grade Heat to Power through closed loop Reverse Electro-Dialysis) - Horizon 2020 programme, Project Number: 640667: www.red-heat-to-power.eu

A Appendix - Modelling equations

A.1 Mass balances

The mass balances for the flow rates F_i [kg_{sol}/s] and the corresponding salt mass fractions w_i [kg_{salt}/kg_{sol}] based on the scheme in Fig. 1 are:

$$F_{high,in} + F_{low,in} = F_{high,out} + F_{low,out} \tag{16}$$

$$F_{high,in} = F_{low,in} \tag{17}$$

$$F_{high,in}\ w_{high,in} + F_{low,in}\ w_{low,in} = F_{high,out}\ w_{high,out} + F_{low,out}\ w_{low,out} \tag{18}$$

$$F_3\ w_{low,out} = F_{low,in}\ w_{low,in} \tag{19}$$

$$F_{high,out}\ w_{high,out} + F_1\ w_{low,out} = F_2\ w_2 \tag{20}$$

$$F_{high,out} + F_1 = F_2 \tag{21}$$

$$F_4 + F_3 = F_{low,in} \tag{22}$$

$$F_{high,in} + F_4 = F_2 \tag{23}$$

A.2 Pitzer model

The Pitzer model is a tool to assess the salt solution thermodynamics needed for modelling the membrane as well as the pressure inside the evaporator.
The osmotic coefficient Φ [-] is assessed through [53]:

$$\Phi - 1 = |z_M z_X| f^{\Phi} + m\left(\frac{2v_X v_M}{v}\right) B^{\Phi}_{MX} + m^2\left(\frac{2(v_M v_X)^{3/2}}{v}\right) C^{\Phi}_{MX} \tag{24}$$

Where m is the molality [mol/kg], z_M and z_X are the charges of the ions [-], v_M and v_X are the number of ions [-]. The other coefficients in eq. (24) are:

$$f^{\Phi} = -A_{\Phi}\left(\frac{I^{1/2}}{1+bI^{1/2}}\right) \tag{25}$$

$$B^{\Phi}_{MX} = \beta^{(0)}_{MX} + \beta^{(1)}_{MX}\ e^{-\alpha_x I^{1/2}} \tag{26}$$

$$I = \frac{1}{2}\sum m_i z_i^2 \tag{27}$$

The coefficients $b = 1.2$ and $\alpha_x = 2$ are constants for all solutes [53]. The ionic strength is represented by I [mol/kg] in eq. (27). The virial coefficients of sodium chloride are $\beta^{(0)}_{MX} = 0.0765$, $\beta^{(1)}_{MX} = 0.2554$ and $C^{\Phi}_{MX} = 0.00127$ [53]. The Debye Hückel coefficient A_{Φ} for water is given in [91, 53]:

$$A_{\Phi} = \frac{1}{3}\left(\frac{2\pi N_0 \rho_w}{1000}\right)^{1/2}\left(\frac{e^2}{DkT}\right)^{3/2} \tag{28}$$

where N_0 is the Avogadro constant [mol^{-1}], k is the Boltzmann constant [$m^2 kg\ s^{-2} K$], e is the electron charge [C] and D the dielectric constant [-] [92]:

$$D = D_{1000} + C\ ln\left(\frac{B+P_{sat}}{B+1000}\right) \tag{29}$$

where P_{sat} is the saturation pressure of water for a given temperature T [K] and the coefficients U_{19} are given in table 6.

$$D_{1000} = U_1\ exp(U_2 T + U_3 T^2) \tag{30}$$

$$C = U_4 + \frac{U_5}{U_6 + T} \tag{31}$$

$$B = U_7 + \frac{U_8}{T} + U_9 T \tag{32}$$

Table 6: Parameters to calculate the dielectric constant of water [92]

U_1	342.8	U_6	−182.9
U_2	$-5.09 \cdot 10^{-3}$	U_7	−8032.5
U_3	$9.47 \cdot 10^{-7}$	U_8	$4.21 \cdot 10^{6}$
U_4	−2.05	U_9	2.14
U_5	3115.9		

The water activity of the solution a_s [-] is correlated to Φ [93]:

$$\Phi = -\left(\frac{1000}{(v_M + v_X) m \tilde{M}}\right) ln(a_s) \tag{33}$$

$$a_s = \frac{P_{sat,sol}}{P_{sat,H_2O}} \tag{34}$$

The boiling point elevation BPE [°C] in the ADRED system is defined as:

$$BPE = T_{evap,vap}(P_{evap,vap}) - T_{sat,H_2O}(P_{evap,vap}) \tag{35}$$

where $P_{evap,vap}$ is the evaporator pressure [bar], $T_{evap,vap}$ is the evaporator temperature [K] and T_{sat,H_2O} is the saturation temperature [K] of pure water at a given pressure. The BPE is needed to assess the pressure in the evaporator, which is reduced compared to pure water due to the presence of NaCl.
The mean activity coefficient of the electrolyte solution γ [-] is required to assess the electricity output from the membrane and can be calculated through the Pitzer correlations [53]:

$$ln(\gamma) = |z_M z_X| f^{\gamma} + m\left(\frac{2v_X v_M}{v}\right) B^{\gamma}_{MX} + m^2\left(\frac{2(v_M v_X)^{3/2}}{v}\right) C^{\gamma}_{MX} \tag{36}$$

$$f^{\gamma} = -A_{\Phi}\left[\frac{I^{1/2}}{1+bI^{1/2}} + \frac{2}{b} ln(1+bI^{1/2})\right] \tag{37}$$

$$B^{\gamma}_{MX} = 2\beta^{(0)}_{MX} + \frac{2\beta^{(0)}_{MX}}{\alpha^2 I}\left[1 - e^{-\alpha I^{1/2}}(1 + \alpha I^{1/2} - (1/2)\alpha^2 I)\right] \tag{38}$$

$$C^{\gamma}_{MX} = \frac{3}{2} C^{\Phi}_{MX} \tag{39}$$

A.3 RED model

Tamburini et al. presented the following, validated RED model including all the membrane specific parameters [50]. Moreover, they optimised the membrane operational variables and this study used the result achieving the highest efficiency.
The volumetric flow rate $\dot{V}$ through the RED membrane [m^3] is defined as:

$$\dot{V} = \varepsilon_{sp}\ N_{cell}\ \delta_{low}\ l\ v \tag{40}$$

where $\varepsilon_{sp} = 0.6$ is the spacer porosity (-), $\delta_{low/high} = 270 \cdot 10^{-6}\ m$ is the high and low compartment thicknesses, $N_{cell} = 50$ number of cell pairs, $v = 0.01$ m/s is the fluid velocity in the membrane and $l = 0.01\ m$ is the length of the membrane [50].
The Nernst equation is required to determine the cell voltage E_{cell} [V]:

$$E_{cell} = (\alpha_{CEM} + \alpha_{AEM})\frac{RT}{F} ln\left(\frac{\gamma_{high} m_{high}}{\gamma_{low} m_{low}}\right) \tag{41}$$

where $F = 96485.3\ C/mol$ is the Faraday constant, $\alpha_{CEM/AEM}$ is the permselectivity of the cation and anion exchange membranes (CEM and AEM) respectively, $m_{high/low}$ is the molality [mol/kg] of the solutions and the equivalent conductivity Λ [S m^2/mol] is obtained through the Jones and Dole equation [94]:

$$\Lambda = \Lambda_0 - \frac{A_{\Lambda} C^{1/2}}{1 + B_{\Lambda} C^{1/2}} - C_{\Lambda} C \tag{42}$$

where C is the molarity [mol/L], $\Lambda_0 = 0.01265\ Sm^2/mol$ [95] and the other parameters were fitted on the experimental results of Chambers et al. [96] by this study: $A_\Lambda = -9.3 \cdot 10^{-3}$, $B_\Lambda = 1.756$, $C_\Lambda = 6.965$.
The electrical resistances $R_{low/high}$ [Ωm^2] of the low and high salinity solutions are given by:

$$R_{low} = s_f \frac{\delta_{low}}{\Lambda_{low} C_{low}} \tag{43}$$

$$R_{high} = s_f \frac{\delta_{high}}{\Lambda_{high} C_{high}} \tag{44}$$

where s_f is the spacer shadow factor [-]. The concentrations $C_{low} = 2\ mol/L$ and $C_{high} = 5\ mol/L$ lead to the highest membrane efficiency [50]. The cell resistance R_{cell} is composed of the resistances of the solutions and the AEM and CEM membrane resistances $R_{AEM} = 2.96 \cdot 10^{-4}\ \Omega m^2$ and $R_{AEM} = 1.55 \cdot 10^{-4}\ \Omega m^2$ [50].

$$R_{cell} = R_{low} + R_{high} + R_{AEM} + R_{CEM} \tag{45}$$

The stack resistance R_{stack}:

$$R_{stack} = N\ R_{cell} + R_{blank} \tag{46}$$

The Open Circuit Voltage OCV

$$OCV = N\ E_{cell} \tag{47}$$

The electrical current density j [A/m^2], where the stack resistance is approximately equal to the load resistance $R_{stack} = R_{ext}$ [50].

$$j = \frac{E_{stack}}{R_{ext}} = \frac{OCV}{2\ R_{stack}} \tag{48}$$

The power per cell pair area P_d [W/m^2] is defined as:

$$P_d = \frac{j^2 R_{ext}}{N} \tag{49}$$

The salt flux through the membrane [mol/(m^{2}s)]:

$$J_{salt} = \frac{j}{F} + \frac{2\ D_{salt}\ (C_{high} - C_{low})}{\delta_m} \tag{50}$$

The outlet concentrations [mol/L] from the membrane can be calculated by the following equation:

$$C_{high,out} = C_{high,in} - \frac{J_{salt}\ A_{cell}}{\dot{V}} \tag{51}$$

$$C_{high,out} = C_{low,in} + \frac{J_{salt}\ A_{cell}}{\dot{V}} \tag{52}$$

The density of sodium chloride solutions [kg/m^3] was measured by Kiepe et al. [97] and fitted

to the following equation by this study:

$$\rho_{sol} = 1133.12 - 0.44\ T + 41.30\ m - 0.024\ m\ T \tag{53}$$

The flow rate specific power output $P_{d,s}$ [W s/kg] is required to assess the overall efficiency of the system and defined by:

$$P_{d,s} = \frac{P_d\ A_{cell}\ N}{\dot{V} \rho_{sol}} \tag{54}$$

A.4 Combining the model components

The adsorption model and the reverse electrodialysis model are the two main building blocks of the model linked by the mass balances as third block. First, the adsorption desalination block runs for 10 cycles to achieve cyclic steady state. Then, the model is connected to the other two system blocks. The average evaporator mass fraction $w_{high,in}$ is passed on to the RED model, which calculates the power production of the membrane and outlet concentrations. These are passed on to the mass balances, which require the distillate production F_4 and the concentrations to calculate the return feed from the membranes to the evaporator.
The output values of the model are SDWP and PR as the two performance indicators of the regeneration side. In addition, the energy efficiency η_{en}, exergy efficiency η_{ex} and power density of silica gel $P_{d,ADRED}$ [W/kg$_{sg}$] are assessed for the overall system and defined by:

$$\eta_{en} = \frac{P_{d,s}\ H_{high,in}\ t_{sim}}{Q_{evap} + Q_{des}} \tag{55}$$

$$\eta_{ex} = \frac{P_{d,s}\ H_{high,in}\ t_{sim}}{Q_{evap}\left(1 - \frac{T_{cond,in}}{T_{evap,in}}\right) + Q_{des}\left(1 - \frac{T_{cond,in}}{T_{ads,in}}\right)} \tag{56}$$

$$P_{d,ADRED} = \frac{P_{d,s}\ F_{high,in}}{M_{sg}} \tag{57}$$

The electric power output $P_{el,ADRED}$ [MW] is a function of η_{en} and the waste heat from the Rankine cycle $\dot{Q}_{wh}$ [MW]:

$$P_{el,ADRED} = \ \eta_{en}\ \dot{Q}_{wh} \tag{58}$$

References

[1] Carey W King, Ashlynn S Holman, and Michael E Webber. Thirst for energy. *Nature Geoscience*, 1(5):283, 2008.

[2] Tyler A. DeNooyer, Joshua M. Peschel, Zhenxing Zhang, and Ashlynn S. Stillwell. Integrating water resources and power generation: The energy–water nexus in illinois. *Applied Energy*, 162:363 – 371, 2016.

[3] Phillip L Gould and Wilfried B Krätzig. Cooling tower structures. handbook of structural engineering. *CRC Press Inc. Boca Raton, FL.*, 1998.

[4] Michelle T.H. van Vliet, Wietse H.P. Franssen, John R. Yearsley, Fulco Ludwig, Ingjerd Haddeland, Dennis P. Lettenmaier, and Pavel Kabat. Global river discharge and water temperature under climate change. *Global Environmental Change*, 23(2):450 – 464, 2013.

[5] Mesfin M Mekonnen and Arjen Y Hoekstra. Four billion people facing severe water scarcity. *Science Advances*, 2(2), 2016.

[6] Michelle TH Van Vliet, John R Yearsley, Fulco Ludwig, Stefan Vögele, Dennis P Lettenmaier, and Pavel Kabat. Vulnerability of us and european electricity supply to climate change. *Nature Climate Change*, 2(9):676, 2012.

[7] Marc A Rosen. Energy-and exergy-based comparison of coal-fired and nuclear steam power plants. *International Journal of Exergy*, 1(3):180–192, 2001.

[8] Alexander S. Rattner and Srinivas Garimella. Energy harvesting, reuse and upgrade to reduce primary energy usage in the usa. *Energy*, 36(10):6172 – 6183, 2011.

[9] G. Venkatesan, S. Iniyan, and Ranko Goic. A prototype flash cooling desalination system using cooling water effluents. *International Journal of Energy Research*, 37(9):1132–1140, 2013.

[10] Mohammed Khennich and Nicolas Galanis. Thermodynamic analysis and optimization of power cycles using a finite low-temperature heat source. *International Journal of Energy Research*, 36(7):871–885, 2012.

[11] Steven Lecompte, Henk Huisseune, Martijn van den Broek, Bruno Vanslambrouck, and Michel De Paepe. Review of organic rankine cycle (orc) architectures for waste heat recovery. *Renewable and Sustainable Energy Reviews*, 47:448 – 461, 2015.

[12] P. J. Yekoladio, T. Bello-Ochende, and J. P. Meyer. Thermodynamic analysis and performance optimization of organic rankine cycles for the conversion of low-to-moderate grade geothermal heat. *International Journal of Energy Research*, 39(9):1256–1271, 2015.

[13] Zhang Shengjun, Wang Huaixin, and Guo Tao. Performance comparison and parametric optimization of subcritical organic rankine cycle (orc) and transcritical power cycle system for low-temperature geothermal power generation. *Applied Energy*, 88(8):2740 – 2754, 2011.

[14] Sylvain Quoilin, Richard Aumann, Andreas Grill, Andreas Schuster, Vincent Lemort, and Hartmut Spliethoff. Dynamic modeling and optimal control strategy of waste heat recovery organic rankine cycles. *Applied Energy*, 88(6):2183 – 2190, 2011.

[15] Ramla Gheith, Fethi Aloui, Mohand Tazerout, and Sassi Ben Nasrallah. Experimental investigations of a gamma stirling engine. *International Journal of Energy Research*, 36(12):1175–1182, 2012.

[16] DW Kirkley. Determination of the optimum configuration for a stirling engine. *Journal of Mechanical Engineering Science*, 4(3):204–212, 1962.

[17] E.D. Rogdakis, G.D. Antonakos, and I.P. Koronaki. Thermodynamic analysis and experimental investigation of a solo v161 stirling cogeneration unit. *Energy*, 45(1):503 – 511, 2012. The 24th International Conference on Efficiency, Cost, Optimization, Simulation and Environmental Impact of Energy, ECOS 2011.

[18] Ulugbek Shaislamov, Yeongmin Kim, Won Sik Kim, Haejun Jeong, Heon-Ju Lee, and Wongee Chun. Hybrid operation of triboelectric nanogenerator for electricity generation by a low-temperature differential heat engine. *International Journal of Energy Research*, 41(10):1412–1421, 2017.

[19] Kai Wang, Seth R. Sanders, Swapnil Dubey, Fook Hoong Choo, and Fei Duan. Stirling cycle engines for recovering low and moderate temperature heat: A review. *Renewable and Sustainable Energy Reviews*, 62:89 – 108, 2016.

[20] Robert L. McGinnis, Jeffrey R. McCutcheon, and Menachem Elimelech. A novel ammonia–carbon dioxide osmotic heat engine for power generation. *Journal of Membrane Science*, 305(1):13 – 19, 2007.

[21] Kerri L. Hickenbottom, Johan Vanneste, Leslie Miller-Robbie, Akshay Deshmukh, Menachem Elimelech, Michael B. Heeley, and Tzahi Y. Cath. Techno-economic assessment of a closed-loop osmotic heat engine. *Journal of Membrane Science*, 535:178 – 187, 2017.

[22] Heru Susanto, Meike Fitrianingtyas, Asep Muhamad Samsudin, and Abdul Syakur. Experimental study of the natural organic matters effect on the power generation of reverse electrodialysis. *International Journal of Energy Research*, 41(10):1474–1486, 2017.

[23] Bruce E Logan and Menachem Elimelech. Membrane-based processes for sustainable power generation using water. *Nature*, 488(7411):313, 2012.

[24] F. Giacalone, C. Olkis, G. Santori, A. Cipollina, S. Brandani, and G. Micale. Novel solutions for closed-loop reverse electrodialysis: thermodynamic characterisation and perspective analysis. *Energy*, 2018.

[25] George Kosmadakis, Michael Papapetrou, Bartolomé Ortega-Delgado, Andrea Cipollina, and Diego-César Alarcón-Padilla. Correlations for estimating the specific capital cost of multi-effect distillation plants considering the main design trends and operating conditions. *Desalination*, 447:74 – 83, 2018.

[26] M. Bevacqua, A. Tamburini, M. Papapetrou, A. Cipollina, G. Micale, and A. Piacentino. Reverse electrodialysis with nh4hco3-water systems for heat-to-power conversion. *Energy*, 137:1293 – 1307, 2017.

[27] Ramato Ashu Tufa, Efrem Curcio, Etienne Brauns, Willem van Baak, Enrica Fontananova, and Gianluca Di Profio. Membrane distillation and reverse electrodialysis for near-zero liquid discharge and low energy seawater desalination. *Journal of Membrane Science*, 496:325–333, 2015.

[28] C. Olkis, G. Santori, and S. Brandani. An adsorption reverse electrodialysis system for the generation of electricity from low-grade heat. *Applied Energy*, 231:222 – 234, 2018.

[29] M. Micari, A. Cipollina, F. Giacalone, G. Kosmadakis, M. Papapetrou, G. Zaragoza, G. Micale, and A. Tamburini. Towards the first proof of the concept of a reverse electrodialysis - membrane distillation heat engine. *Desalination*, 453:77 – 88, 2019.

[30] Noel Dow, Stephen Gray, Jun de Li, Jianhua Zhang, Eddy Ostarcevic, Audra Liubinas, Paul Atherton, Gareth Roeszler, Andrew Gibbs, and Mikel Duke. Pilot trial of membrane distillation driven by low grade waste heat: Membrane fouling and energy assessment. *Desalination*, 391:30 – 42, 2016. Advances in Membrane Des: Keynotes from MEMDES 2-Singapore.

[31] Zisheng Lu and Ruzhu Wang. Experimental and simulation analysis of low temperature heat sources driven adsorption air conditioning, refrigeration, integrating ammonia, and organic expanding power generation. *International Journal of Energy Research*, 42(13):4157–4169, 2018.

[32] J. Bauer, R. Herrmann, W. Mittelbach, and W. Schwieger. Zeolite/aluminum composite adsorbents for application in adsorption refrigeration. *International Journal of Energy Research*, 33(13):1233–1249, 2009.

[33] Kyaw Thu, Bidyut Baran Saha, Anutosh Chakraborty, Won Gee Chun, and Kim Choon Ng. Study on an advanced adsorption desalination cycle with evaporator–condenser heat recovery circuit. *International Journal of Heat and Mass Transfer*, 54(1):43–51, 2011.

[34] Kyaw Thu, Hideharu Yanagi, Bidyut Baran Saha, and Kim Choon Ng. Performance investigation on a 4-bed adsorption desalination cycle with internal heat recovery scheme. *Desalination*, 402:88 – 96, 2017.

[35] Hongkuan Zhang, Hongting Ma, Sihan Liu, Hao Wang, Yuexia Sun, and Daokun Qi. Investigation on the operating characteristics of a pilot-scale adsorption desalination system. *Desalination*, 473:114196, 2020.

[36] Aung Myat, Ng Kim Choon, Kyaw Thu, and Young-Deuk Kim. Experimental investigation on the optimal performance of zeolite–water adsorption chiller. *Applied Energy*, 102:582 – 590, 2013. Special Issue on Advances in sustainable biofuel production and use - XIX International Symposium on Alcohol Fuels - ISAF.

[37] B.B Saha, A Akisawa, and T Kashiwagi. Solar/waste heat driven two-stage adsorption chiller: the prototype. *Renewable Energy*, 23(1):93 – 101, 2001.

[38] Seong-Yong Woo, Ho-Saeng Lee, Ho Ji, Deok-Soo Moon, and Young-Deuk Kim. Silica gel-based adsorption cooling cum desalination system: Focus on brine salinity, operating pressure, and its effect on performance. *Desalination*, 467:136 – 146, 2019.

[39] Sourav Mitra, Kyaw Thu, Bidyut Baran Saha, and Pradip Dutta. Performance evaluation and determination of minimum desorption temperature of a two-stage air cooled silica gel/water adsorption system. *Applied Energy*, 206:507 – 518, 2017.

[40] Quanwen Pan, Jiajie Peng, Hongbin Wang, Haiquan Sun, and Ruzhu Wang. Experimental investigation of an adsorption air-conditioner using silica gel-water working pair. *Solar Energy*, 185:64 – 71, 2019.

[41] Suxin Qian, Kyle Gluesenkamp, Yunho Hwang, Reinhard Radermacher, and Ho-Hwan Chun. Cyclic steady state performance of adsorption chiller with low regeneration temperature zeolite. *Energy*, 60:517 – 526, 2013.

[42] Angelo Freni, Alessio Sapienza, Ivan S. Glaznev, Yuriy I. Aristov, and Giovanni Restuccia. Experimental testing of a lab-scale adsorption chiller using a novel selective water sorbent "silica modified by calcium nitrate". *International Journal of Refrigeration*, 35(3):518 – 524, 2012. Refrigeration and Heat Pumping with Sorption Processes.

[43] Jun W. Wu, Mark J. Biggs, and Eric J. Hu. Dynamic model for the optimisation of adsorption-based desalination processes. *Applied Thermal Engineering*, 66(1):464 – 473, 2014.

[44] C.J. Chen, R.Z. Wang, Z.Z. Xia, J.K. Kiplagat, and Z.S. Lu. Study on a compact silica gel–water adsorption chiller without vacuum valves: Design and experimental study. *Applied Energy*, 87(8):2673 – 2681, 2010.

[45] C.Y. Tso, K.C. Chan, Christopher Y.H. Chao, and C.L. Wu. Experimental performance analysis on an adsorption cooling system using zeolite 13x/cacl2 adsorbent with various operation sequences. *International Journal of Heat and Mass Transfer*, 85:343 – 355, 2015.

[46] Ahmed S. Alsaman, Ahmed A. Askalany, K. Harby, and Mahmoud S. Ahmed. Performance evaluation of a solar-driven adsorption desalination-cooling system. *Energy*, 128:196 – 207, 2017.

[47] Alessio Sapienza, Giuseppe Gullì, Luigi Calabrese, Valeria Palomba, Andrea Frazzica, Vincenza Brancato, Davide La Rosa, Salvatore Vasta, Angelo Freni, Lucio Bonaccorsi, and Gaetano Cacciola. An innovative adsorptive chiller prototype based on 3 hybrid coated/granular adsorbers. *Applied Energy*, 179:929 – 938, 2016.

[48] Raya AL-Dadah, Saad Mahmoud, Eman Elsayed, Peter Youssef, and Fadhel Al-Mousawi. Metal-organic framework materials for adsorption heat pumps. *Energy*, 190:116356, 2020.

[49] Peter G. Youssef, Hassan Dakkama, Saad M. Mahmoud, and Raya K. AL-Dadah. Experimental investigation of adsorption water desalination/cooling system using cpo-27ni mof. *Desalination*, 404:192 – 199, 2017.

[50] A. Tamburini, M. Tedesco, A. Cipollina, G. Micale, M. Ciofalo, M. Papapetrou, W. Van Baak, and A. Piacentino. Reverse electrodialysis heat engine for sustainable power production. *Applied Energy*, 206(Supplement C):1334 – 1353, 2017.

[51] C. Olkis, S. Brandani, and G. Santori. Performance and cycle analysis of a small-scale adsorption desalinator. *Submitted to Energy*, 2019.

[52] Kim Choon Ng, Kyaw Thu, Youngdeuk Kim, Anutosh Chakraborty, and Gary Amy. Adsorption desalination: An emerging low-cost thermal desalination method. *Desalination*, 308:161 – 179, 2013. New Directions in Desalination.

[53] Kenneth S Pitzer and Guillermo Mayorga. Thermodynamics of electrolytes. ii. activity and osmotic coefficients for strong electrolytes with one or both ions univalent. *The Journal of Physical Chemistry*, 77(19):2300–2308, 1973.

[54] Hisham T El-Dessouky and Hisham Mohamed Ettouney. *Fundamentals of salt water desalination*. Elsevier, 2002.

[55] Q.W. Pan, R.Z. Wang, and L.W. Wang. Comparison of different kinds of heat recoveries applied in adsorption refrigeration system. *International Journal of Refrigeration*, 55:37 – 48, 2015.

[56] V. Palomba, B. Dawoud, A. Sapienza, S. Vasta, and A. Frazzica. On the impact of different management strategies on the performance of a two-bed activated carbon/ethanol refrigerator: An experimental study. *Energy Conversion and Management*, 142:322 – 333, 2017.

[57] Giulio Santori, Alessio Sapienza, and Angelo Freni. A dynamic multi-level model for adsorptive solar cooling. *Renewable Energy*, 43(Supplement C):301 – 312, 2012.

[58] Kyaw Thu, Kim Choon Ng, Bidyut B Saha, Anutosh Chakraborty, and Shigeru Koyama. Operational strategy of adsorption desalination systems. *International Journal of Heat and Mass Transfer*, 52(7):1811–1816, 2009.

[59] A. Freni, G. Maggio, S. Vasta, G. Santori, F. Polonara, and G. Restuccia. Optimization of a solar-powered adsorptive ice-maker by a mathematical method. *Solar Energy*, 82(11):965 – 976, 2008.

[60] M. M. Dubinin and V. A. Astakhov. Development of the concepts of volume filling of micropores in the adsorption of gases and vapors by microporous adsorbents. *Bulletin of the Academy of Sciences of the USSR, Division of Chemical Science*, 20(1):3–7, Jan 1971.

[61] Giulio Santori and Chiara Di Santis. Optimal fluids for adsorptive cooling and heating. *Sustainable Materials and Technologies*, 12:52 – 61, 2017.

[62] Donald G Archer and Richard W Carter. Thermodynamic properties of the nacl+ h2o system. 4. heat capacities of h2o and nacl (aq) in cold-stable and supercooled states. *The Journal of Physical Chemistry B*, 104(35):8563–8584, 2000.

[63] Duong D Do. *Adsorption Analysis: Equilibria and Kinetics:(With CD Containing Computer Matlab Programs)*, volume 2. World Scientific, 1998.

[64] C. Olkis, S. Brandani, and G. Santori. Design and experimental study of a small scale adsorption desalinator. *Applied Energy*, 253:113584, 2019.

[65] G. Santori, A. Frazzica, A. Freni, M. Galieni, L. Bonaccorsi, F. Polonara, and G. Restuccia. Optimization and testing on an adsorption dishwasher. *Energy*, 50:170 – 176, 2013.

[66] Alessio Sapienza, Andreas Velte, Ilya Girnik, Andrea Frazzica, Gerrit Füldner, Lena Schnabel, and Yuri Aristov. "water - silica siogel" working pair for adsorption chillers: Adsorption equilibrium and dynamics. *Renewable Energy*, 110(Supplement C):40 – 46, 2017.

[67] VDI-Gesellschaft Verfahrenstechnik und Chemieingenieurwesen (VDI-GVC). Wärmeatlas, vdi 10. auflage, 2006.

[68] Jun W Wu, Eric J Hu, and Mark J Biggs. Thermodynamic cycles of adsorption desalination system. *Applied Energy*, 90(1):316–322, 2012.

[69] Patricia Palenzuela, Ashraf S Hassan, Guillermo Zaragoza, and Diego-C Alarcón-Padilla. Steady state model for multi-effect distillation case study: Plataforma solar de almería med pilot plant. *Desalination*, 337:31–42, 2014.

[70] Xiaolin Wang, Kim Choon Ng, Anutosh Chakarborty, and Bidyut Baran Saha. How heat and mass recovery strategies impact the performance of adsorption desalination plant: Theory and experiments. *Heat Transfer Engineering*, 28(2):147–153, 2007.

[71] Phillip Bendix, Gerrit Füldner, Marc Möllers, Harry Kummer, Lena Schnabel, Stefan Henninger, and Hans-Martin Henning. Optimization of power density and metal-to-adsorbent weight ratio in coated adsorbers for adsorptive heat transformation applications. *Applied Thermal Engineering*, 124:83 – 90, 2017.

[72] A. Askalany, C. Olkis, E. Bramanti, D. Lapshin, L. Calabrese, E. Proverbio, A. Freni, and G. Santori. Silica-supported ionic liquids for heat-powered sorption desalination. *ACS Applied Materials & Interfaces*, 11(40):36497–36505, 2019. PMID: 31512475.

[73] Animesh Pal, Maisara Shahrom Raja Shahrom, Muhammad Moniruzzaman, Cecilia Devi Wilfred, Sourav Mitra, Kyaw Thu, and Bidyut Baran Saha. Ionic liquid as a new binder for activated carbon based consolidated composite adsorbents. *Chemical Engineering Journal*, 326:980 – 986, 2017.

[74] Frank J. Millero, Rainer Feistel, Daniel G. Wright, and Trevor J. McDougall. The composition of standard seawater and the definition of the reference-composition salinity scale. *Deep Sea Research Part I: Oceanographic Research Papers*, 55(1):50 – 72, 2008.

[75] Sibnath Kayal, Sun Baichuan, and Bidyut Baran Saha. Adsorption characteristics of aqsoa zeolites and water for adsorption chillers. *International Journal of Heat and Mass Transfer*, 92:1120 – 1127, 2016.

[76] Andrea Frazzica and Vincenza Brancato. Verification of hydrothermal stability of adsorbent materials for thermal energy storage. *International Journal of Energy Research*, 43(12):6161–6170, 2019.

[77] Peter G Youssef, Saad M Mahmoud, and Raya K Al-Dadah. Performance analysis of four bed adsorption water desalination/refrigeration system, comparison of aqsoa-z02 to silica-gel. *Desalination*, 375:100–107, 2015.

[78] J. W. Post, C. H. Goeting, J. Valk, S. Goinga, J. Veerman, H. V. M. Hamelers, and P. J. F. M. Hack. Towards implementation of reverse electrodialysis for power generation from salinity gradients. *Desalination and Water Treatment*, 16(1-3):182–193, 2010.

[79] Eman Elsayed, AL-Dadah Raya, Saad Mahmoud, Paul A Anderson, Ahmed Elsayed, and Peter G Youssef. Cpo-27 (ni), aluminium fumarate and mil-101 (cr) mof materials for adsorption water desalination. *Desalination*, 406:25–36, 2017.

[80] Eman Elsayed, Raya AL-Dadah, Saad Mahmoud, Paul Anderson, and Ahmed Elsayed. Experimental testing of aluminium fumarate mof for adsorption desalination. *Desalination*, 475:114170, 2020.

[81] C. Olkis, H. Dong, S. Brandani, and G. Santori. Ionogels at the water energy nexus for desalination powered by ultra low grade heat. *Environmental Science & Technology*, 54(6):3591–3598, 2020.

[82] Hongsheng Dong, Ahmed A. Askalany, Christopher Olkis, Jiafei Zhao, and Giulio Santori. Hydrothermal stability of water sorption ionogels. *Energy*, 189:116186, 2019.

[83] Quanwen Pan, Jiajie Peng, and Ruzhu Wang. Experimental study of an adsorption chiller for extra low temperature waste heat utilization. *Applied Thermal Engineering*, 163:114341, 2019.

[84] S.K. Henninger, G. Munz, K.-F. Ratzsch, and P. Schossig. Cycle stability of sorption materials and composites for the use in heat pumps and cooling machines. *Renewable Energy*, 36(11):3043 – 3049, 2011.

[85] Wilhelm Dengler and W Krückels. Untersuchung über die kinetik der adsorption von wasserdampf an einzelkörnern technischer adsorbentien. *Chemie Ingenieur Technik*, 43(5):269–271, 1971.

[86] Michele Tedesco, Andrea Cipollina, Alessandro Tamburini, I. David L. Bogle, and Giorgio Micale. A simulation tool for analysis and design of reverse electrodialysis using concentrated brines. *Chemical Engineering Research and Design*, 93:441 – 456, 2015.

[87] Adam M. Weiner, Ronan K. McGovern, and John H. [Lienhard V]. Increasing the power density and reducing the levelized cost of electricity of a reverse electrodialysis stack through blending. *Desalination*, 369:140 – 148, 2015.

[88] L. Gurreri, A. Tamburini, A. Cipollina, G. Micale, and M. Ciofalo. Cfd prediction of concentration polarization phenomena in spacer-filled channels for reverse electrodialysis. *Journal of Membrane Science*, 468:133 – 148, 2014.

[89] Harrison J. Cassady, Emily C. Cimino, Manish Kumar, and Michael A. Hickner. Specific ion effects on the permselectivity of sulfonated poly(ether sulfone) cation exchange membranes. *Journal of Membrane Science*, 508:146 – 152, 2016.

[90] A. Zlotorowicz, R.V. Strand, O.S. Burheim, Ø. Wilhelmsen, and S. Kjelstrup. The permselectivity and water transference number of ion exchange membranes in reverse electrodialysis. *Journal of Membrane Science*, 523:402 – 408, 2017.

[91] Leonard F Silvester and Kenneth S Pitzer. Thermodynamics of electrolytes. 8. high-temperature properties, including enthalpy and heat capacity, with application to sodium chloride. *The Journal of Physical Chemistry*, 81(19):1822–1828, 1977.

[92] Daniel J Bradley and Kenneth S Pitzer. Thermodynamics of electrolytes. 12. dielectric properties of water and debye-hueckel parameters to 350. degree. c and 1 kbar. *Journal of physical chemistry*, 83(12):1599–1603, 1979.

[93] Bert R Staples and Ralph L Nuttall. The activity and osmotic coefficients of aqueous calcium chloride at 298.15 k. *Journal of Physical and Chemical Reference Data*, 6(2):385–408, 1977.

[94] Grinnell Jones and Malcolm Dole. The electrical conductance of aqueous solutions of barium chloride as a function of the concentration. *Journal of the American Chemical Society*, 52(6):2245–2256, 1930.

[95] SS Islam, RL Gupta, and K Ismail. Extension of the falkenhagen-leist-kelbg equation to the electrical conductance of concentrated aqueous electrolytes. *Journal of Chemical and Engineering Data*, 36(1):102–104, 1991.

[96] J. F. Chambers, Jean M. Stokes, and R. H. Stokes. Conductances of concentrated aqueous sodium and potassium chloride solutions at 25°. *The Journal of Physical Chemistry*, 60(7):985–986, 1956.

[97] Jörn Kiepe, Anne Karine de Araújo Rodrigues, Sven Horstmann, and Jürgen Gmehling. Experimental determination and correlation of liquid density data of electrolyte mixtures containing water or methanol. *Industrial & Engineering Chemistry Research*, 42(9):2022–2029, 2003.